Molecular design and fabrication of PIM-1/polyphosphazene blend membranes with high performance for CO_2/N_2 separation

Ali K. Sekizkardes[a,b],* Samir Budhathoki[a,b],* Lingxiang Zhu[a,b], Victor Kusuma[a,b], Zi Tong[a,b], Joshua S. McNally[c], Janice A. Steckel[a], Shouliang Yi[a,b] and David Hopkinson[a]

*Email: ali.sekizkardes@netl.doe.gov, Phone: (412) 386-7255

*Email: samir.budhathoki@netl.doe.gov, Phone(412)-386-7337

a. U.S. Department of Energy National Energy Technology Laboratory, Pittsburgh, PA 15236
b. NETL Support Contractor, Pittsburgh, PA 15236, United States
c. Idaho National Laboratory, Idaho Falls, ID 83415, United States

Keywords: Molecular Dynamic simulations, PIM-1, polymer blend membranes, CO2 separation

Abstract

New polymeric blend membranes for CO_2 separation were synthesized based on insights from molecular dynamics simulation.. A molecular-level structure-property relationship in polymers of intrinsic microporosity (PIM) based blend membranes, was investigated in detail computationally. Calculated local density profiles and energy of interaction of the blend membranes, composed of PIM-1 and various polyphosphazenes, showed that using the polyphosphazene with a higher concentration of ether side chains can improve the compatibility with PIM-1. Based on the findings of computational studies, blend membranes were experimentally fabricated from PIM-1 and polyphosphazenes with various polyether side chain concentrations. Polyether concentration in polyphosphazenes was correlated with the film properties and gas transport performance of the blend membranes. Blend membranes showed very high CO_2 permeability (3100-5300barrer) and improved CO_2/N_2 selectivity (24-28), outperforming all other PIM-based blend membranes reported to date. Moreover, the CO_2 permeability performance of the blend membranes was tested 566 hours under real post-combustion flue gas from a coal-fired power plant, including CO_2, N_2, H_2O, O_2, SO_x and NO_x.

1. Introduction

CO_2 capture using gas separation membranes has attracted ever-increasing research, competing with sorbent- and solvent-based CO_2 separation technologies.[1] Particularly, polymeric membranes have been prevalent in CO_2 separation for various applications such as post-combustion flue gas separation.[2] Polymeric membranes offer attractive properties such as low-cost, scalability, film flexibility, high gas permeability and selectivity. Designing a polymeric membrane that shows highly selective CO_2 permeability is imperative to achieve an economically viable separation process. Film-forming properties and the processability of membranes should also translate into a scalable material. Polymers of intrinsic microporosity (PIMs), specifically PIM-1, are an accrescent class of polymeric membranes. Unlike most conventional polymers, PIM-1 is constructed from contorted and rigid monomers, creating micropores and mesopores within the polymer.[3] The unique polymer structure of PIM-1 proffers high free volume for small gas molecules, such as CO_2, to diffuse with high flux. On the other hand, PIM-1 shows moderate CO_2/N_2 selectivity (14-17) due to its average pore size distribution (1-2 nm) and relatively large microporosity. Lower pore size distribution in porous polymers usually results in low CO_2 solubility. Thus, PIM-1 sits just below the 2008 Robeson upper bound for CO_2/N_2 separation in the high permeability regime, which is generally used as an empirical upper limit for permeability and selectivity of polymer membranes.[4, 5] Recently, studies have focused on advancing CO_2/N_2 selectivity of PIM-1. These studies can be divided into two categories: 1) Post-synthetic functionalization of PIM-1 with functional groups such as carboxylic acid, amidoxime, amine and tetrazole. These functional groups generally render higher CO_2 affinity compared to nitrile functional groups in PIM-1. 2) Blending PIM-1 with other highly selective polymers. Although both methods bring some degree of improvement to CO_2/N_2 selectivity, functionalization of PIM-1, in general, has some drawbacks such as brittle film formation, limited solubility, and scalability. Apart from functionalization and blending categories, PIM-1-based mixed matrix membranes (MMMs), using fillers such as metal organic frameworks (MOFs) and porous organic polymers (POPs), have also emerged as a viable option. However, CO_2/N_2 selectivity in mixed matrix membranes has been reported to either drop or show only incremental improvement.[6]

A considerable literature body has been accumulated recently on blending PIM-1 with highly CO_2 selective polymers such as Matrimid, Torlon, Ultem and polyethylene glycol (PEG).[7] Accordingly, some degree of CO_2/N_2 selectivity improvement has been achieved with these blend membranes. Moreover, the blend membranes have shown an advantage in processability because the blending-polymers are soluble in common solvents. This suggests that blend membranes can be used in MMM studies to boost the gas transport properties further. However, the polymers used for blending with PIM-1 generally suffer from very low CO_2 permeability compared to PIM-1, which diminishes the overall CO_2 permeability of the blend membranes. Another problem arises from poor compatibility between the blending-polymer and PIM-1. For example, a higher concentration of Matrimid (>10%) in PIM-1 can further improve CO_2/N_2 separation properties.[8] However, at these concentrations, phase separation between Matrimid and PIM-1 becomes more apparent, often resulting in poor mechanical properties.

Recently, our group reported a new type of blend membrane based on PIM-1 and [2-(2-methoxyethoxy)ethoxy]-co-(*p*-methoxyphenoxy) polyphosphazene (MEEP80) (Table 1).[9] Reported PIM-1/MEEP80 blend membranes not only provided a better gas transport performance compared to neat PIM-1, but the mechanical properties of the blend membrane were superior as well. The polymer structure of polyphosphazene consists of a flexible phosphazene backbone with a low rotational energy barrier from P=N bonding. Given the flexibility of the polymer chains, MEEP80 does not show crystalline domains that limit CO_2 diffusivity as in other polyether-based polymers such as PEG. Thus, the CO_2 permeability of polyphosphazene can reach up to 250 barrer with high CO_2/N_2 selectivity of over 40. [10]

Although our initial study showed the potential of having promising blend membranes based on PIM-1 and MEEP80, there is still a need for a better blend formulation to achieve higher gas transport performance by investigating molecular-level interaction between these two polymers, which is yet to be dissected in detail.

Here, we present the fabrication and characterization of new blend membranes based on PIM-1 and polyphosphazene. Blend membranes were designed computationally and molecular-level compatibility between PIM-1 and polyphosphazene was investigated by molecular dynamic simulations. Based on the findings of computational studies, blend membranes were cast into dense films and tested under mixed gas permeation settings. Moreover, we also report the CO_2 separation performance of the blend membranes tested under post-combustion flue gas from a coal-fired power plant.

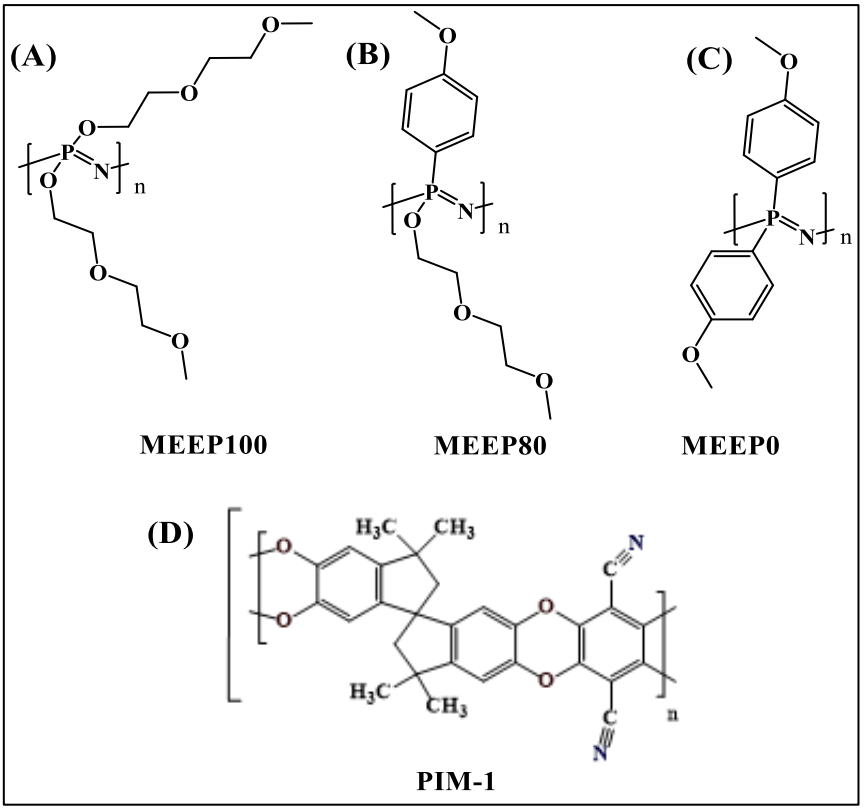

Figure 1. Polymer structure illustration of (A) MEEP100, (B) MEEP80, (C) MEEP0 and (D) PIM-1.

Table 1. Functional groups and their concentration in polyphosphazenes: MEEP0, MEEP80 and MEEP100.

Polyphosphazene	MEE: 2-(2-methoxyethoxy)ethoxy]	p-methoxyphenoxy	o-allylphenoxy
MEEP0	0 %	97%	3%
MEEP80	80%	17%	3%
MEEP100	100%	0%	0%

2. Experimental Methods and Materials

2.1 Membrane fabrication

The synthesis of the materials was performed according to previously reported methods including polymers; MEEP [10], MEEP80 [9], [11], MEEP0 [12] and PIM-1 [9], [13].

As-synthesized polymers were dissolved in chloroform solution (2wt% polymer) as 10wt% and 25wt% polyphosphazene with respect to PIM-1. Homogenous solutions were filtered and then cast in poly(tetrafluoroethylene) (PTFE) molds and the solvent was evaporated at room temperature overnight. Without any treatment with other solvents, membranes were removed from the PTFE molds and thermally activated at 70 ^{o}C for 2 hours under vacuum.

2.2 Mixed gas permeation test

Mixed-gas permeability was measured using an in house-built isobaric (constant pressure and variable volume) gas permeation system at 22 ^{o}C. The permeation cell was designed to provide countercurrent flow of the feed and sweep gases. A Viton® o-ring was used to mount the film sample in the permeation cell, exposing an active area of 0.67 cm^2 for gas permeation. 20 mol% CO_2, 20 mol% N_2 and argon was used in the gas mixture on a dry basis, and the total feed flow was maintained at 10 mL/min using a digital mass flow controller (Alicat Scientific) Ultra-high purity argon was used as the sweep gas at about 4.5 mL/min. The pressure was maintained at 1.6 and 1.3 bar for the feed and sweep sides, respectively, measured with a pressure transducer (Honeywell). The permeate flow rate was measured using a mass flow meter. The gas composition of the retentate and permeate streams were characterized by a gas chromatograph (Perkin Elmer ARNEL Clarus 500). The permeability, *P*i, of a particular gas species *i* is defined as

(1)

where *A* is the effective area of the film for gas permeation, $p_{2,i}$ and $p_{1,i}$ are the partial pressure of gas component *A* in the feed and permeate sides, respectively, *S* is the flow rate of the sweep gas,

and x_i and x_{sweep} are the mole fraction of gas component *i* and sweep gas (argon in this study) in the sweep-out stream, respectively. *l* is the film thickness at 50 – 90 μm, measured by a caliper micrometer (Mitutoyo). For each condition, 5 measurements were carried out after reaching the steady state. Selectivity, α of gas species *i* with respect to species *j* is

(2)

3. Blend Polymer Molecular Dynamic Simulations

3.1 Polymer models: determination of chain lengths and construction

Polymer blend membranes were computationally designed based on PIM-1 and three different polyphosphazenes: MEEP100, MEEP80 and MEEP0. These polyphosphazenes consist of the same phosphazene backbone (-P=N-), but they differ from each other as to the pendant groups substituted on the phosphazene backbone, as illustrated in Figure 1. The concentration of the polyether side groups in polyphosphazenes was altered from 0% for MEEP0 to 80% and 100% for MEEP80 and MEEP100, respectively. It is not feasible to simulate these polymers at full size using all atomistic force-fields in molecular dynamics (MD) because they are large molecules with hundreds of thousands of repeat units. Therefore, it is crucial to calculate the minimum chain length that represents a polymer with a large molecular weight. To achieve this goal, the solubility parameters of PIM-1 and MEEP polymers were calculated for various numbers of repeat units. The molecular size at which the solubility parameter reaches a near-constant value is said to represent the real polymer chain [14]. We used a simulation methodology to calculate solubility parameters that has been published previously and shown to be accurate [15].

The Polymer builder and Amorphous cell modules in Materials Studio software [16] were used to build polymer chains of PIM-1, MEEP100, MEEP80 and MEEP0 with 5 to 60 repeat units and generate initial configurations with low density, 0.1 g/cc to 0.8 g/cc. Since PIM-1 is a ladder-like polymer with no single backbone, the methodology to build such polymers is not implemented in the Polymer builder module. Therefore, the procedure by Heuchel et. al. [17] was followed to construct PIM-1 polymer chains. For all polymer systems, chains were terminated by non-polar methyl groups. To calculate the solubility parameter, two polymer chains with the same repeat units were inserted in a cubic box. Bond lengths, bond angles, charges, dihedral, and improper force field parameters along with the Lennard-Jones (LJ) parameters for van der Waals interactions were derived from the all-atomistic class I CVFF (consistent valence force field) [18].

3.2 Equilibration procedures

PIM-1 is a rigid polymer with a limited number of conformations which prevents it from being packed efficiently into a simulation box. Therefore, PIM-1 was subjected to a series of annealing, compression and relaxation steps based on a scheme developed by Larsen et al. [19]. LAMMPS [20] MD software was used to obtain the system density at 313 K and 1 bar. The Nosé–Hoover thermostat with a damping factor of 0.1 ps, was used for the temperature control [21] and the pressure of the system was kept constant by utilizing the extended Lagrangian [22] approach.

Polyphosphazenes, on the other hand, are rubbery polymers and therefore, the compression and relaxation scheme was not performed for MEEP100, MEEP80 or MEEP0. All the systems were equilibrated for 5 ns in NPT (constant number, constant pressure, and constant temperature) ensemble at 1 bar 313 K. Solubility parameters were computed from 100 configurations generated by equilibrated NPT runs. The results for PIM-1 and MEEP100 are shown in Figure 2.

3.3 Molecular dynamics simulations

For structural characterization, molecular dynamics simulations were performed for seven different systems: MEEP100, MEEP80, MEEP0, PIM-1, PIM-1/MEEP100 blend, PIM-

1/MEEP80 blend and PIM-1/MEEP0 blend at 313 K and 1 bar pressure. To study the blends, the systems were composed of 25 mol% of the polyphosphazene polymers. For MD simulation of pure polymers, four polymer chains were included in the model. For the blend systems, two MEEP100, two MEEP80 or two MEEP0 polymers were used for every six polymer chains of PIM-1 to maintain 25 mol% polyphosphazene. In terms of weight percent, the systems were 17 wt% MEEP100, 15 wt% MEEP80 and 19 wt% MEEP0, respectively. As mentioned above, PIM-1 and PIM-1 based blend systems were prepared using a compression and relaxation scheme by Larsen et. al. The Lennard-Jones and electrostatic interactions were truncated at 14 Å. The particle–particle particle–mesh Ewald method was used to control long range electrostatic interactions [23]. All systems were equilibrated for 10 to 40 ns in the NPT ensemble. The last one ns of the equilibrated trajectory was used for structural characterization at 313 K and 1 bar. The results are averaged over four to eight independent simulations.

The pore size distributions (PSDs) were computed from 400 configurations from four independent simulations of the equilibrated trajectories using the methodology developed by Gelb and Gubbins [24] implemented in molecular simulation software RAPSA (v2.0) [25].

4. Results

4.1 Solubility Parameter

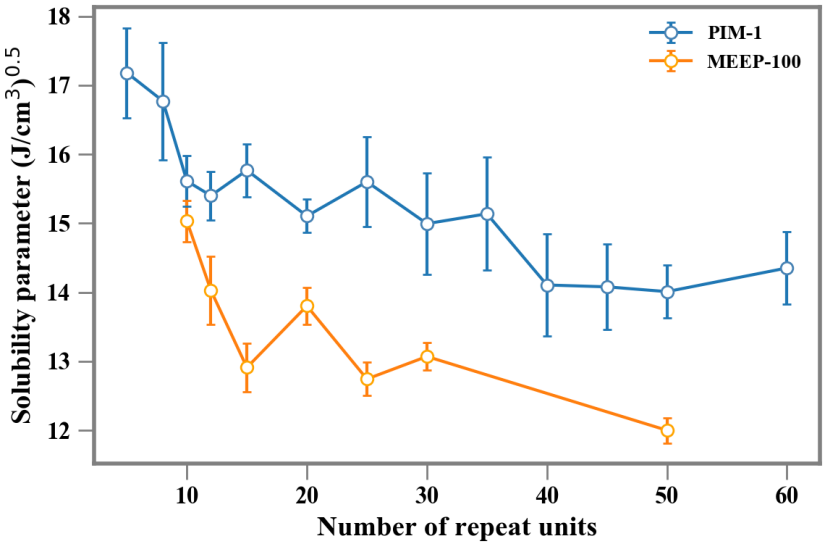

Figure 2: Solubility parameter for PIM-1 and MEEP100 as a function of number of repeat units.

It is observed that the solubility parameter is nearly constant after 15 repeat units for MEEP100 and 30 repeat units for PIM-1. Therefore, to study the gas transport and structural properties of MEEP100 and PIM-1 polymers using MD simulation, polymer chains of at least 15 and 30 (respectively) repeat units are required. Since MEEP80 and MEEP0 are synthesized by aroxyl functionalization of MEEP100 and are closely related, solubility parameters were not computed for those polymer systems and the minimum number of repeat units required was assumed to be

15. For this study, MEEP100, MEEP80 and MEEP0 polymers with 30, 26 and 32 (respectively) repeat units and PIM-1 with 30-35 repeat units were created.

4.2 Simulated Density and Free Volume Fraction

The bulk density of each polymer was determined by dividing the mass of the polymer by the volume of the simulation box. The computed densities are shown in Figure 3.

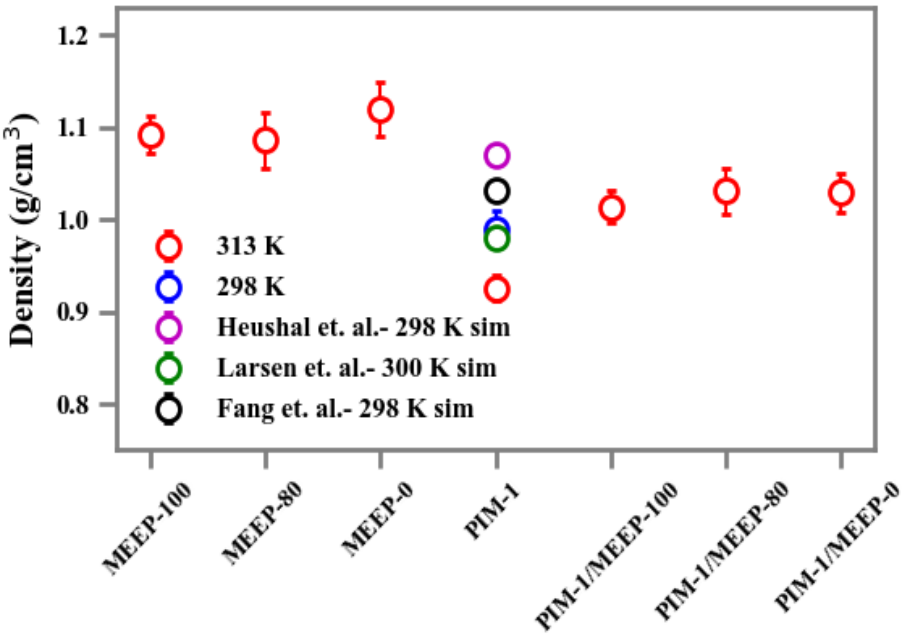

Figure 3. Simulated bulk densities of pure and blend polymers at 313 K and 1 bar. PIM-1 density at 298 K and 1 bar is compared with the simulation data from published reports [17],[19],[26].

Polyphosphazenes have larger densities than PIM-1 and blends because they are rubbery polymers and pack efficiently. We obtained a PIM-1 density of (0.925 ± 0.005) g/cm^3 at 313 K. For a direct comparison of our simulation results with the available published simulated values, we computed the PIM-1 density at 298 K. Our results are in excellent agreement with the simulated bulk density result obtained by Larsen et. al. [19] at 298 K and are in reasonable agreement with other simulation studies [17],[26],[27] that have reported PIM-1 densities ranging from 0.8 to 1.07 g/cm^3. For glassy polymers such as PIM-1, experimental densities are reported in terms of skeletal density that discounts the pore volume (ρ_{skel} = m/ (V_{tot} – V_{pore})) [27]. Approximating the pore volume based on the fractional free volume (details below), we obtained the skeletal density of 1.29 ± 0.03 g/cm^3. Thus, experimentally measured values (0.94 to 1.4 g/cm^3) [17], [28], [29] are in a similar range with the calculated skeletal density. Polymer blends have densities between the polyphosphazenes and PIM-1. Since MEEP80, MEEP0 and PIM/MEEP blends are a new class of polymers, the simulation densities are not available in the literature for comparison.

PIM-1 is a porous glassy polymer and large free-volume is one of its defining structural characteristics, responsible for its high gas permeance [30], [31]. Therefore, our simulation model was further characterized in terms of fractional free volume to validate the choice of force-field used for this study. Free volume was calculated based on a method to calculate excluded volume [32] [33], in which the simulation box was divided into cubelets of length 1 Å. A cubelet was considered occupied if the distance between the center of the cubelet and any polymer atom was less than the hardcore radius of any atom, $r_{ev} = s\,(\sigma_i/2 + r_{probe})$, in which σ_i is the van der Waals radius for the atom of the polymer, s is the scaling factor and r_{probe} is the radius of the probe atom

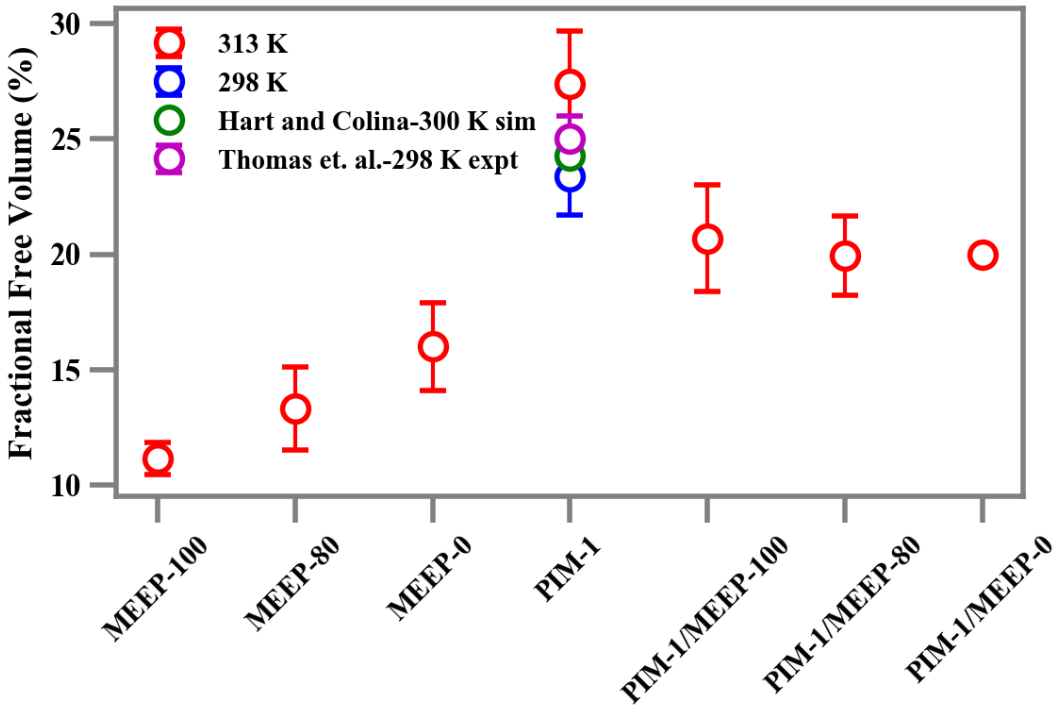

set equal to 1.0 Å.

Figure 4. Fractional free volume of pure and blend polymers at 313 K and 1 bar. PIM-1 free volume at 298 K and 1 bar is compared with the simulation [34] and experimental [35] data.

A scaling factor of 0.8 was chosen for this study to be consistent with Shah and Maginn [33]. For each of the configurations, a list of cubelets was generated to record whether the cubelet is occupied or unoccupied . The free volume fraction was calculated to be f_{ev} = number of unoccupied cubelets/total number of cubelets. The free volume fraction of each system is shown in Figure 4.

In Figure 4, it is observed that pure PIM-1 polymer has a large free volume fraction of about 27% at 313 K. The free volume fraction at 298 K was computed to be 23.4 ± 1.7% which agrees very well with the values reported in the literature [34], [35] that range between 24-26%. MEEP100 has a free volume fraction of 12%, the lowest of the polyphasphazenes included in this study. The free volume fraction of MEEP80 is 14%. The higher free volume fraction of MEEP80 (with respect to MEEP100) can be attributed to the replacement of 20% of the methoxyethoxy groups by bulky allyl-phenoxy and methoxyphenoxy functional groups. The free volume fraction of MEEP0 is

increased further, to 16%, which can be attributed to the replacement of all pendant ether groups by bulky phenoxy groups.

The polymer blends, as expected, have larger free-volume fraction compared to pure polyphosphazene polymers but are slightly smaller than pure PIM-1. The marginal decrease in the free-volume fraction of blend polymers compared to PIM-1 is due to the presence of 25 mol% polyphosphazene rubbery polymers that can, to some extent, pack into the large pores of PIM-1.

4.2 Simulated Pore Size Distributions

Simulated, average pore size distributions (PSDs) for PIM-1, MEEP100, MEEP80, MEEP0 and blends of these polymers are presented in Figure 5. The calculated results for PIM-1 are in excellent qualitative and quantitative agreement with previous simulation studies. For example, the PSD calculated in this work for PIM-1 closely resembles that previously calculated by Larsen et al. [19], as well as that calculated by Gonciaruk et al. [27], with a peak near 0.3 nm and a shoulder towards larger pore sizes.

Pore size distributions were measured experimentally via positron annihilation lifetime spectroscopy (PALS) for PIM-1, several polyphosphazenes, and their blends [9]. While there are qualitative similarities between the simulated and experimentally measured PSDs, there are quantitative differences. Specifically, the simulations tend to predict a lower peak pore size than was observed using PALS. For example, for PIM-1 the experimentally measured PSD displays a peak near 1 nm, which is significantly larger than the peak at 0.3 nm predicted by the simulations. Also, the experimental PSD for MEEP80 predicts a unimodal peak near 0.7 nm while the simulated PSD exhibited a peak near 0.1 nm with a significant shoulder at larger diameters. For these polymers, the peaks in the simulated PSD are significantly lower than the peaks in their experimentally measured PSDs.

Comparison between simulated pore size distributions and experimentally measured PSDs is not straightforward. The derivation of the PSD from experimental data is subject to a very sensitive dependence on assumptions and models used [36]. In addition, while the derivation of the PSD from simulation data is straightforward, the construction and equilibration of the simulation model are far from simple, depend on many assumptions with notable sensitivity, and are not realistic in terms of the size of the molecules included. In this work, simulation models consisted of 26 to 35 polymer repeat units in the simulation, when, in reality, the polymers are large molecules that consist of hundreds of thousands of repeat units. Therefore, it perhaps should not be surprising that the simulations, consisting as they do of chains that are significantly shorter than the real polymer chains, do not render PSDs in quantitative agreement with the experiment.

Based on the simulated pore size distributions, a comparison between the pores of the neat polyphosphazenes, PIM-1 and their blends is possible. MEEP100 exhibits a pore size of 0.1 nm, the smallest of the polymers simulated in this work, which is consistent with the flexible nature of the polyphosphazene backbone and MEE side chains. The introduction of bulky phenoxy side groups in MEEP80 and MEEP0 is associated with a very slight increase in the dominant pore size as well as a noticeable increase in the shoulder at around 0.7 nm. The incorporation of polyphosphazenes into PIM-1 decreases the intensity of the dominant peak, a qualitative feature

that is in agreement with the experiment.[9] Additionally, the dominant pore size changes from 0.3 nm for PIM-1 to about 0.2 nm for the PIM-1/polyphosphazene blends.

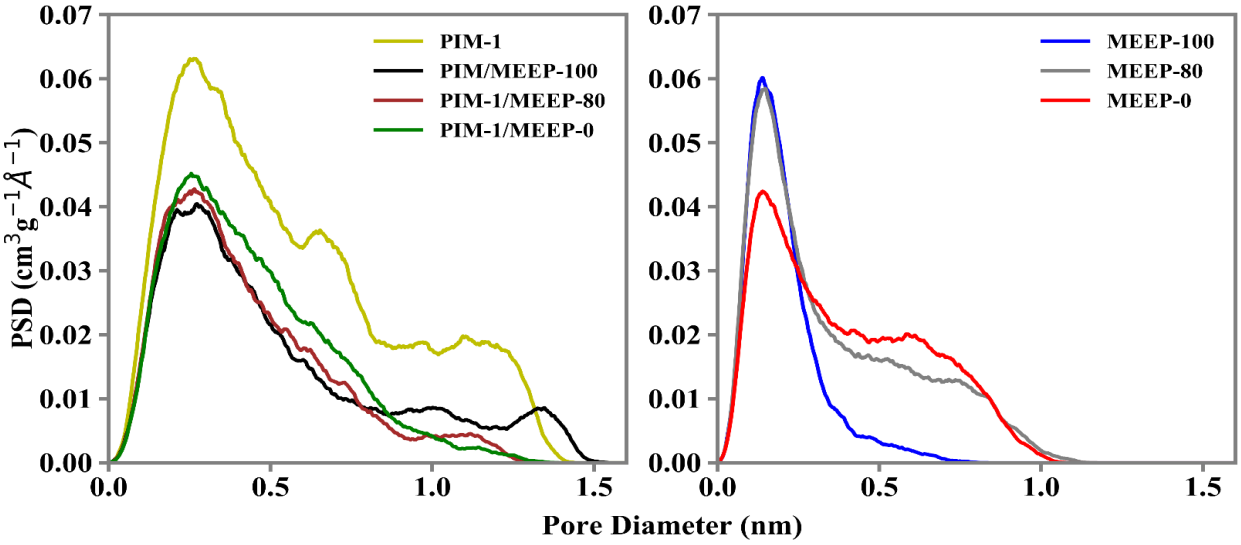

Figure 5. Simulated pore size distributions of pure and blend polymers at 313 K and 1 bar.

4.3 Local Density Profiles and Interaction Energy

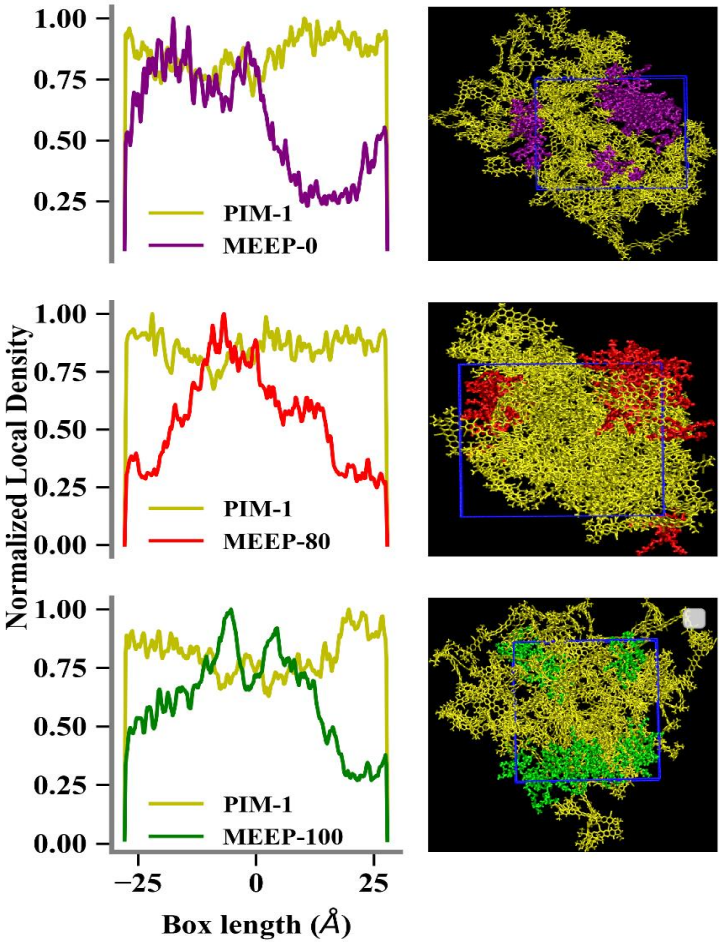

Figure 6. Local density profiles of PIM-1/25% MEEP0 (yellow/purple), PIM-1/25%MEEP80 (yellow/red) and PIM-1/25% MEEP100 blends (yellow/green). To the right of the density profiles are snapshots of the blends from the simulations. The color of the polymers in the snapshots corresponds to the colors in the density profiles.

Polymer compatibility in blends is a critical property. Good blend membranes are characterized by effective mixing between the blending polymers such that the membranes are homogeneous. To assess the homogeneity and structural features of the blends, local density profiles of the blends were computed across box lengths (Figure 6). The local density profiles reported in Figure 6 were averaged over x, y, and z dimensions of a simulation box. There is a noticeable difference in the local density profiles of the two polymers. The normalized local density of PIM-1 in all the blend polymers remains comparatively steady within a density range of about 0.75 to 1. The polyphosphazenes, on the other hand, show large variations in density when blended with PIM-1. MEEP0, MEEP80 and MEEP100 density profiles show that most of the polyphosphazenes are concentrated in a certain region of the box featured by a large peak, leaving other regions with negligible densities, also visible in the accompanying snapshot from simulation. This shows that there is a tendency for the flexible backbone and ether side chains of the polyphosphazenes to

aggregate together in local clusters. Such aggregation could contribute to phase separation that could be detrimental to the overall membrane integrity. Local density profiles can provide qualitative insight on the spatial arrangement of the molecules but cannot quantitatively characterize the degree of phase separation or homogeneity present in the three different PIM-1/MEEP blends. To understand the likelihood of aggregation of polyphosphazenes, PIM-1-polyphosphazene and polyphosphazene-polyphosphazene interaction energies were computed for all the blends. The results are listed in Table 2.

Table 2: Energy of interaction of PIM-1 and polyphosphazene polymer molecules. Interaction energies were normalized by molar volume.

Blends	Interaction energy (PIM-1-MEEP) (kJ/m^3)	Interaction energy (MEEP-MEEP) (kJ/m^3)
PIM-1/MEEP0	-139 ± 14	-222 ± 16
PIM-1/MEEP80	-128 ± 10	-176 ± 13
PIM-1/MEEP100	-130 ± 5	-152 ± 5

The energies of interaction show that, for all the blends, the interaction between the PIM-1 and MEEP is weaker than the MEEP-MEEP self-interactions. The PIM-1-polyphosphazene interaction in PIM-1/MEEP0, PIM-1/MEEP100 and PIM-1/MEEP80 is the same within statistical uncertainty. Intermolecular interactions for polyphosphazenes, however, are larger for MEEP0 followed by MEEP80 and MEEP100 which suggest that MEEP0 has a large tendency towards self-aggregation followed by MEEP80 and MEEP100. This observation is in line with a previous study on the functionalized polyphosphazene which suggests that polyphosphazene functionalized with aroxyl functional groups have a high tendency of aggregation [37]. Since PIM-1/MEEP interactions are similar for all the blends, the membrane integrity is determined by the intermolecular interaction strength of the polyphosphazenes. MEEP100 has the weakest self-interaction energy amongst the phosphazenes, and therefore it is likely to yield a relatively homogeneous blend membrane with a lower chance of phase separation compared to the blends synthesized from functionalized phosphazenes.

4.4 Membrane fabrication and characterization

Following the MD simulation studies, blend membranes based on PIM-1 and poylphosphazenes were experimentally fabricated. Three polyphosphazenes: MEEP100, MEEP80 and MEEP0 were blended (10 wt% and 25 wt%) in PIM-1 and cast into ~80 mm dense films. Membrane films were characterized by FTIR to examine the functional groups of each blending polymer. Characteristic FT-IR absorption stretching of PIM-1 was found at 2250 cm^{-1} and 1008 cm^{-1} for nitrile (-CN) and dioxane (C-O-C) groups, respectively[38]. Polyphosphazene content in blend membranes can be

verified from P-O-C peaks at 1200 and 1046 cm^{-1}, which are not present in neat PIM-1 (Figure 7)[39].

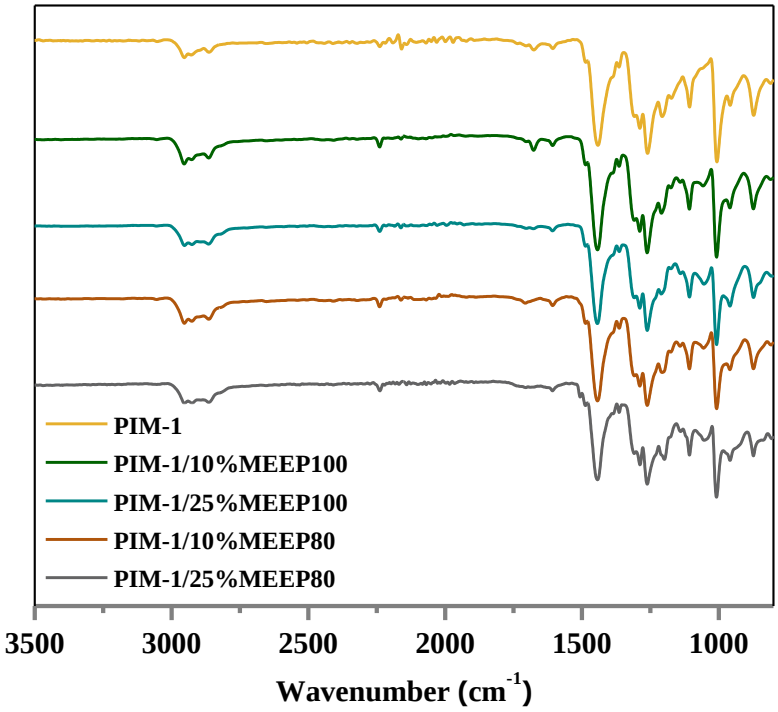

Figure 7. Full FT-IR spectrum (3500-750 cm^{-1}) of neat PIM-1, PIM-1/10%MEEP100, PIM-1/25%MEEP100, PIM-1/10%MEEP80 and PIM-1/25%MEEP80.

The membrane composition was further characterized by energy-dispersive X-ray (EDX) mapping. EDX is an important instrumental tool to analyze the distribution of polyphosphazene in PIM-1, as phosphorous elements can only be found in one of the blending polymers. Phosphorous mapping of PIM-1/10%MEEP100, PIM-1/10%MEEP80 and PIM-1/10%MEEP0 is shown in Figure 8. Despite the possible existence of micro-phase separation, MEEP100 (Figure 8A) and MEEP80 (Figure 8B) based membranes showed uniform distribution of phosphorous across the membranes. In contrast, PIM-1/10%MEEP0 had both phosphorous rich and lean regions with an area usually greater than 100 μm^2 as shown in the EDX mapping of Figure 8C, indicating macro-phase separation occurs to MEEP0 and PIM-1. Due to this severe macro-phase separation, a bubble-like structure was formed on the surface of a PIM-1/MEEP0 bulk film (Figure 8C). This is consistent with the poor compatibility between MEEP0 and PIM-1 which was revealed by MD simulations in Section 4.3. PIM-1 is a microporous polymer, which has a pore size distribution between 0.9 and 1.1 nm. It is possible that relatively flexible polyphosphazenes can partially intercalate into pores of PIM-1 through the polyether side chain. However, this intercalation can be impeded when the polyphosphazene is substituted with bulkier phenoxy groups. This trend was observed both experimentally and computationally.

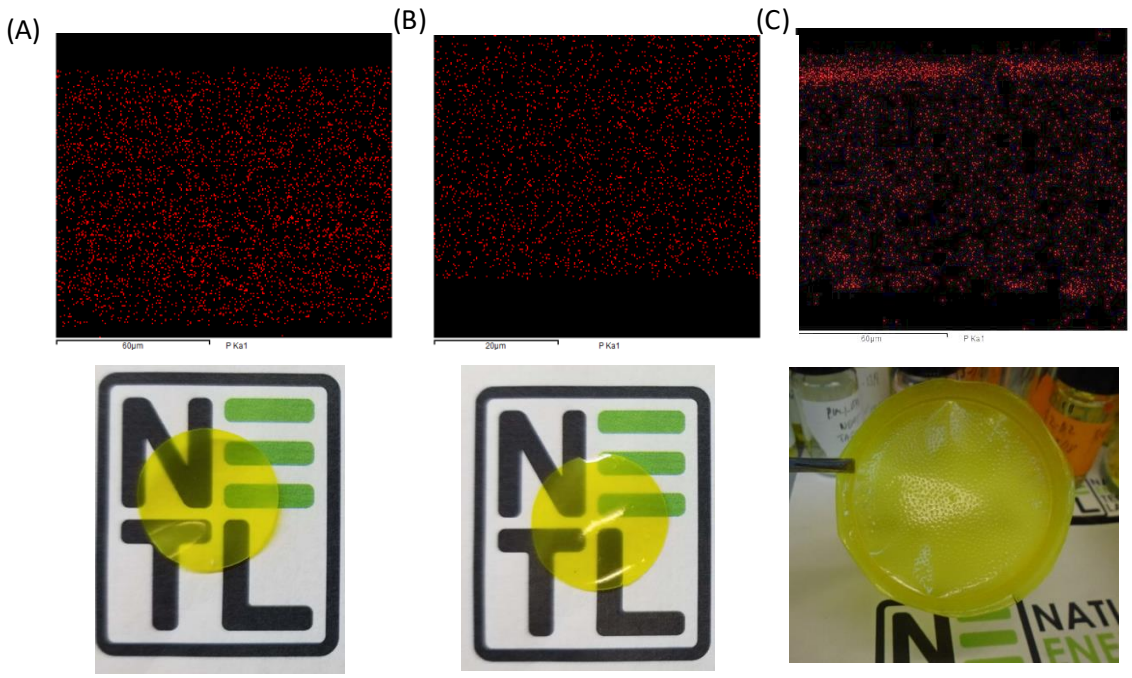

Figure 8. EDX phosphorous mapping of membrane cross-sections and membrane images for **(**A) PIM-1/10%MEEP100 (B) PIM-1/10%MEEP80 and (C) PIM-1/10%MEEP0.

As-cast membranes based on PIM-1/MEEP100 and PIM-1/MEEP80 showed uniform film formation. On the other hand, membranes based on PIM-1/MEEP0 exhibited an apparent phase separation, a trend that was generally predicted by MD simulations (Figure 8).

4.5. Mixed gas permeation test

Gas transport properties of blend membranes were characterized by using 20 mol% CO_2/20 mol% N_2/balance Ar mixed gas at 22 ^oC. The CO_2 permeability of neat PIM-1 was calculated as 7210 barrer with a CO_2/N_2 selectivity of 18, which is in line with the literature.[5] PIM-1/10%MEEP80 and PIM-1/25%MEEP80 both had CO_2 permeabilities of around 3100 barrer which is lower than the permeability of neat PIM-1. However, CO_2/N_2 selectivity properties of these two blend membranes were improved by up to 40% (Figure 9). In the literature, blending highly permeable polymers, including PIM-1, with less permeable polymers results in reduced CO_2 permeability in the blend material. [40] Following the same trend, MEEP100 based membranes also showed CO_2/N_2 selectivity enhancement at the expense of CO_2 permeability (Figure 9).

However, the CO_2 permeability of PIM-1/10%MEEP100 was substantially higher than any of the other blends tested, at 5200 barrer. Remarkably, the CO_2/N_2 selectivity of PIM-1/10%MEEP100 (24) was comparable with PIM-1/10%MEEP80 (also 24), despite higher CO_2 permeability. It is noteworthy that this PIM-1 blend results in gas separation properties that are on or above the Robeson upper bound using both MEEP80 and MEEP100, which is unusual compared to other

literature reports, and in fact the performance of these blends exceeds all other reported PIM-1 blends to date (Figure 10). The superior gas transport performance of MEEP100 based blend membranes compared with MEEP80 can be attributed to a higher concentration of ether side chains. Previous studies have also noted that the higher content of MEE groups will enhance the CO_2 permeability of polyphosphazenes due to a higher CO_2 affinity compared to the phenoxy groups.[10] Also, because MEEP 100 does not contain the bulky phenoxy groups that are present in MEEP 80, MEEP100 can better intercalate into the pores of PIM-1 contributing to better polymer-polymer interaction and CO_2/N_2 separation properties. Lowering the pore size in polymers provides more surface energy for polar gasses, hence leading to higher CO_2/N_2 selectivity [5]. This is further supported by computational results which suggest better compatibility of MEEP100 with PIM-1 compared to MEEP80 and MEEP0.

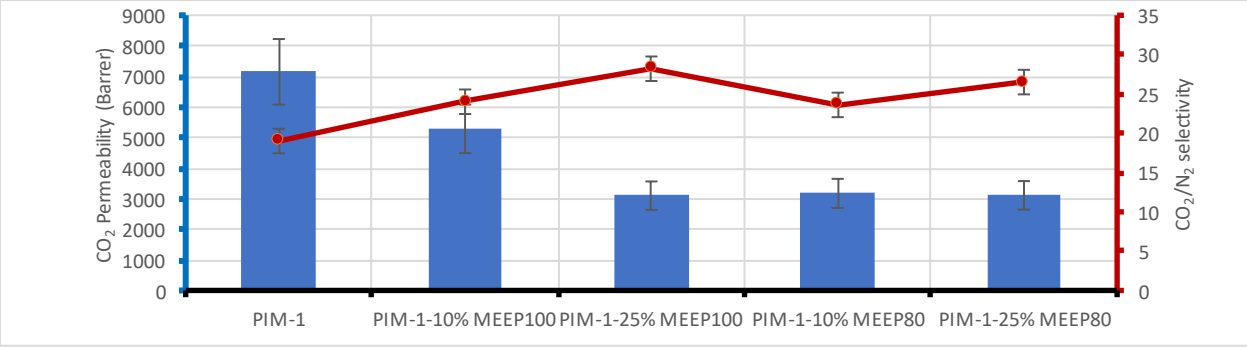

Figure 9. CO_2 permeability and CO_2/N_2 of PIM-1, PIM-1/10%MEEP100, PIM-1/25%MEEP100, PIM-1/10%MEEP80 and PIM-1/10%MEEP80. PIM-1/MEEP0 based blend formed defective films and were not included in the gas permeation test.

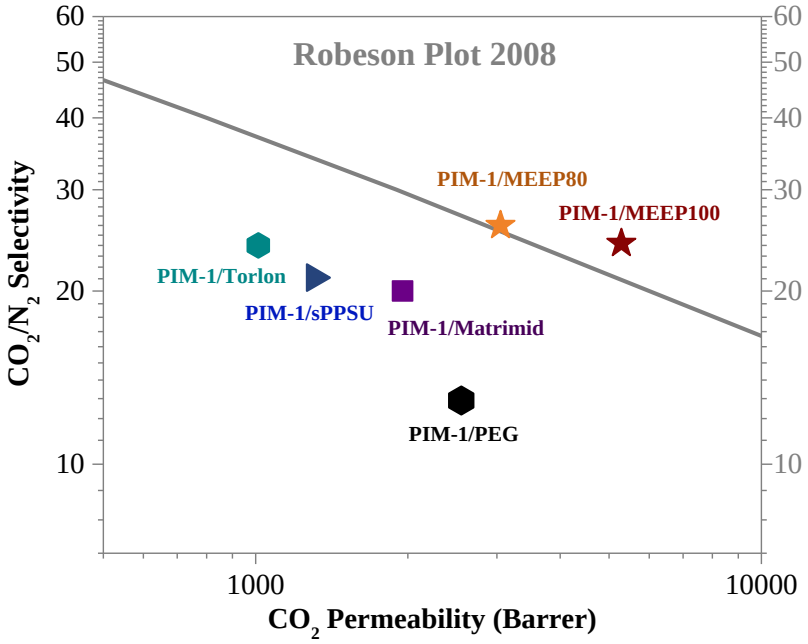

399

400 **Figure 10.** CO_2 permeability and CO_2/N_2 selectivity of PIM-1/10%MEEP80 and PIM-
401 1/10%MEEP100 and other reported blend membranes.

402

403 ## 4.6. Gas permeation test under actual power plant flue gas

404 We tested the gas transport performance of one of the blend membranes (PIM-1/25%MEEP80)
405 using real flue gas from a coal-fired power plant. This testing capability was designed by our group
406 using an isobaric (constant pressure) gas permeation system [38] stationed at the National Carbon
407 Capture Center (NCCC) in Wilsonville, Alabama. The actual flue gas contains humidity, SOx and
408 NOx. The flue gas feed is composed of approximately 80% N_2, 10% CO_2, 9% O_2, 10 ppm NO_2
409 and 1.3 ppm SO_2, similar to a previous study reported by our group.[9] The membrane was
410 maintained at 40 °C. CO_2, H_2O, N_2 and O_2 permeability for the PIM-1/25%MEEP80 during a 566-
411 hour long experiment are shown in Figure 11. PIM-1/25%MEEP80 showed a high CO_2
412 permeability of 3000 barrer. The selectivity of CO_2 over N_2 was calculated as 21. The CO_2/N_2
413 selectivity was reduced compared to lab testing due to a higher temperature and the presence of
414 moisture. The gas transport properties of PIM-1/25%MEEP80 using flue gas are consistent with
415 mixed gas permeability testing when the aging properties of the membrane, presence of moisture,
416 and temperature differences between tests (40 °C at NCCC vs. 22 °C in the lab) are considered.
417 The membrane films tested at NCCC had aged for approximately 6 months before they were tested,
418 but this did not notably reduce the high CO_2 permeability performance of the membranes.
419 However, membranes tested had a thickness of around 80 mm. A thin film PIM-1 blend is expected
420 to exhibit more significant aging.

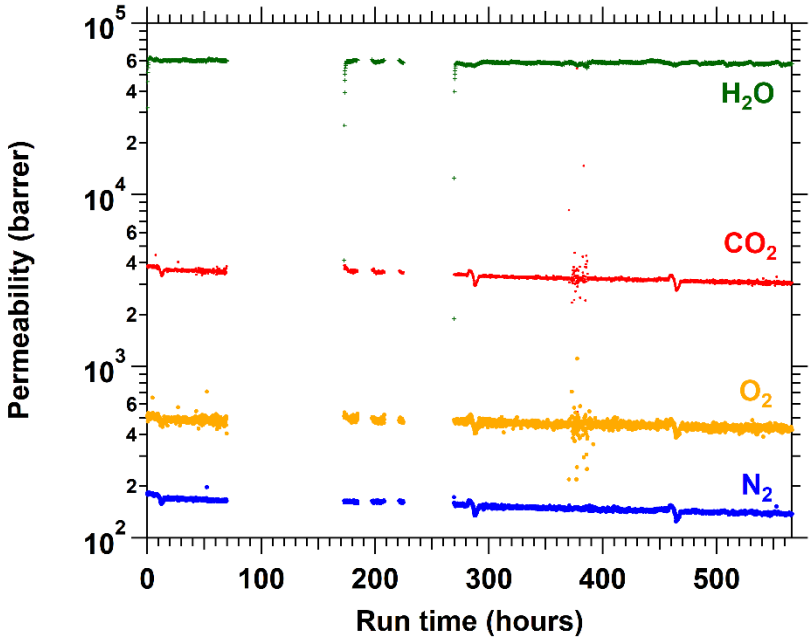

Figure 11. Gas permeability test of PIM-1/25%MEEP80 under a coal-fired flue gas mixture including H_2O, CO_2, O_2 and N_2. Gaps in data are due to various process and analytical instrument outages.

5. Conclusions

PIM-1/polyphosphazenes blend membranes were designed and fabricated with varying degrees of polyether functionalization in the polyphosphazene component. MD simulations were used to investigate the compatibility between PIM-1 and the blending-polymer, polyphosphazene. MD simulations showed that a higher concentration of polyether side chains in the polyphosphazene polymer provides more favorable compatibility with PIM-1. In light of the MD simulation results, polyphosphazenes were synthesized with a high polyether content (MEEP80 and MEEP100) and blended with PIM-1. Overall, the blend membranes showed 24-48% CO_2/N_2 selectivity improvement compared to neat PIM-1. Particularly, the polyphosphazene, MEEP100 blend membranes exhibited very high CO_2 permeability (5340 barrer), with a CO_2/N_2 selectivity of 24. PIM-1/10%MEEP100 and PIM-1/10%MEEP80 membranes perform on or above the 2008 Robeson upper bound, and are substantially better than any other PIM-1 blend membrane that has been reported to date.

Disclaimer

This project was funded by the United States Department of Energy, National Energy Technology Laboratory, in part, through a site support contract. Neither the United States Government nor any agency thereof, nor any of their employees, nor the support contractor, nor any of their employees, makes any warranty, express or implied, or assumes any legal liability or responsibility for the accuracy, completeness, or usefulness of any information, apparatus, product, or process disclosed, or represents that its use would not infringe privately owned rights. Reference herein to any specific commercial product, process, or service by trade name, trademark, manufacturer, or otherwise does not necessarily constitute or imply its endorsement, recommendation, or favoring by the United States Government or any agency thereof. The views and opinions of authors expressed herein do not necessarily state or reflect those of the United States Government or any agency thereof.

References

[1] K. Xie, Q. Fu, G.G. Qiao, P.A. Webley, Journal of Membrane Science, 572 (2019) 38-60.

[2] T.C. Merkel, H. Lin, X. Wei, R. Baker, Journal of Membrane Science, 359 (2010) 126-139.

[3] N.B. McKeown, P.M. Budd, Chemical Society Reviews, 35 (2006) 675-683.

[4] L.M. Robeson, Journal of Membrane Science, 320 (2008) 390-400.

[5] Z.-X. Low, P.M. Budd, N.B. McKeown, D.A. Patterson, Chemical Reviews, (2018).

[6] N. Prasetya, N.F. Himma, P.D. Sutrisna, I.G. Wenten, B.P. Ladewig, Chemical Engineering Journal, (2019) 123575.

[7] C. Ma, J.J. Urban, Proceedings of the Nature Research Society, 2 (2018) 02002.

[8] W.F. Yong, F.Y. Li, Y.C. Xiao, P. Li, K.P. Pramoda, Y.W. Tong, T.S. Chung, Journal of Membrane Science, 407 (2012) 47-57.

[9] A.K. Sekizkardes, V.A. Kusuma, J.S. McNally, David W. Gidley, K. Resnik, S.R. Venna, D. Hopkinson, Journal of Materials Chemistry A, 6 (2018) 22472-22477.

[10] C. J. Orme, M. K. Harrup, T. A. Luther, R. P. Lash, K. S. Houston, D. H. Weinkauf and F. F. Stewart,

Journal of Membrane Science, 186, (2001), 249–256.

[11] V.A. Kusuma, J.S. McNally, J.S. Baker, Z. Tong, L. Zhu, C.J. Orme, F.F. Stewart, D.P. Hopkinson, ACS Applied Materials & Interfaces, 12 (2020) 30787-30795.

[12] R.E. Singler, G.L. Hagnauer, N.S. Schneider, B.R. Laliberte, R.E. Sacher, R.W. Matton, Journal of Polymer Science: Polymer Chemistry Edition, 12 (1974) 433-444.

[13] P.M. Budd, E.S. Elabas, B.S. Ghanem, S. Makhseed, N.B. McKeown, K.J. Msayib, C.E. Tattershall, D. Wang, Advanced Materials, 16 (2004) 456-459.

[14] M. Zhang, P. Choi, U. Sundararaj, Polymer, 44 (2003) 1979-1986.

[15] I. M. de Arenaza, E. Meaurio, J. R. Sarasua, A. D. S. Gomes (Ed.), Polymerization, InTech (2012), 10.5772/51327.

[16] Dassault Systèmes BIOVIA, Materials Studio, v8.0.100.21, San Diego: Dassault Systèmes, 2014

[17] M. Heuchel, D. Fritsch, P.M. Budd, N.B. McKeown, D. Hofmann, Journal of Membrane Science, 318 (2008) 84-99.

[18] P. Dauber-Osguthorpe, V. A. Roberts, D. J. Osguthorpe, J. Wolff, M. Genest, A. T. Haggler, Proteins, 4 (1998) 31-47.

[19] G.S. Larsen, P. Lin, K.E. Hart, C.M. Colina, Macromolecules, 44 (2011) 6944-6951

[20] S. Plimpton, Journal of Computational Physics, 117 (1995) 1-19.

[21] W.G. Hoover, Physical Review A, 31 (1985) 1695-1697.

[22] W. Shinoda, M. Shiga, M. Mikami, Physical Review B, 69 (2004) 134103.

[23] R. W. Hockney, J. W. Eastwood, Computer Simulation Using Particles, Taylor and Francis, Bristol, PA, 1988.

[24] L.D. Gelb, K.E. Gubbins, Langmuir, 15 (1999) 305-308.

[25] D. Dubbeldam, S. Calero, D. E. Ellis, R. Q. Snurr, Molecular Simulation, 42 (2016) 81-101.

[26] W. Fang, L. Zhang, J. Jiang, Molecular Simulation, 36 (2010) 992-1003.

[27] A. Gonciaruk, K. Althumayri, W.J. Harrison, P.M. Budd, F.R. Siperstein, Microporous and Mesoporous Materials, 209 (2015) 126-134.

[28] N.B. McKeown, B. Gahnem, K.J. Msayib, P.M. Budd, C.E. Tattershall, K. Mahmood, S. Tan, D. Book, H.W. Langmi, A. Walton, Angewandte Chemie International Edition, 45 (2006) 1804-1807.

[29] G.S. Larsen, P. Lin, F.R. Siperstein, C.M. Colina, Adsorption, 17 (2011) 21-26.

[30] N.B. McKeown, P.M. Budd, Macromolecules, 43 (2010) 5163-5176.

[31] N. Du, H.B. Park, G.P. Robertson, M.M. Dal-Cin, T. Visser, L. Scoles, M.D. Guiver, Nature Materials, 10 (2011) 372-375.

[32] G. L. Deitrick, L. E. Scriven, H. T. Davis, Journal of Chemical Physics, 90 (1989) 2370-2385.

[33] J.K. Shah, E.J. Maginn, The Journal of Physical Chemistry B, 109 (2005) 10395-10405.

[34] K.E. Hart, C.M. Colina, Journal of Membrane Science, 468 (2014) 259-268.

[35] S. Thomas, I. Pinnau, N. Du, M.D. Guiver, Journal of Membrane Science, 333 (2009) 125-131.

[36] G. Kupgan, T. P. Liyana-Arachchi, C. M. Colina, Langmuir, 33 (2017), 11138-11145.

[37] H. R. Allcock, C. J. Nelson, W. D. Coggio, I. Manners, W. J. Koros, D. R. B. Walker, L. A. Pessan, Macromolecules 26 (1993) 1493-1502.

[38] A.K. Sekizkardes, V.A. Kusuma, G. Dahe, E.A. Roth, L.J. Hill, A. Marti, M. Macala, S.R. Venna, D. Hopkinson, Chemical Communications, 52 (2016) 11768-11771.

[39] D. Ucan, F.E. Kanik, Y. Karatas, L. Toppare, Sensors and Actuators B: Chemical, 201 (2014) 545-554.

[40] W.F. Yong, Z.K. Lee, T.-S. Chung, M. Weber, C. Staudt, C. Maletzko, ChemSusChem, 9 (2016) 1953-1962.